Fire Technology, 55, 981–1012, 2019

https://doi.org/10.1007/s10694-019-00815-x

Fire Smoke Transport and Opacity Reduced-Order Model (Fire-STORM): A New Computer Model for High-Rise Fire Smoke Simulations

Serhat Bilyaz and Ofodike A. Ezekoye, Department of Mechanical Engineering, The University of Texas at Austin, Austin, TX 78712, USA*

Received: 14 June 2018/**Accepted:** 8 January 2019

Abstract. The problem of smoke spread through elevator shafts in high rise buildings is analyzed theoretically and numerically in this paper. While experiments and computational fluid dynamics (CFD) models have been used for such exercises, there is a need for fast reduced-order models for such scenarios. Towards this goal, a transient network model called High-rise fire smoke transport and opacity reduced-order model (Fire-STORM) was developed to investigate heat and mass transfer through the elevator shaft during fires. The model numerically solves the coupled set of differential equations of the fire floor in conjunction with the steady state conservation equations of the elevator shaft. The model is validated in two stages. First, the stack effect in a non-fire scenario is analyzed. Pressure differences through exterior doors and elevator doors are compared with experimental data available in the literature and results of a computational fluid dynamics tool. Then, a first-floor fire scenario is considered for the same high-rise building in four different cases which are combinations of different building tightness and ambient temperatures. The results are compared with CFD simulations. For the four different building envelope and ambient thermal conditions, the soot mass fractions and optical visibilities were calculated and compared to CFD predictions. Overall, Fire-STORM is a simple and fast tool to model the evolution of heat and mass transfer in a high-rise building affected by fire. While Fire-STORM is excellent in predicting transient smoke transport for buildings with loose envelopes, it should be used with caution for buildings with tight envelopes since the errors for these cases are relatively high. Despite this, the relative computational speed difference between Fire-STORM and the CFD model highlights the utility of a reduced-order model for firefighter decision making and building control system design.

Keywords: Fire, Smoke, High-rise, CFD, Model, Transport, Opacity

List of symbols

α	Thermal diffusivity
α_f	Fire growth rate
C_d	Discharge coefficient

* Correspondence should be addressed to: Ofodike A. Ezekoye, E-mail: dezekoye@mail.utexas.edu

c_p	Constant pressure specific heat
c_v	Constant volume specific heat
δ_p	Thermal penetration depth
g	Gravity
H	Room height
h_c	Convective heat transfer coefficient
h_r	Radiative heat transfer coefficient
h_t	Total heat transfer coefficient
Δh_c	Heat of combustion
k	Thermal conductivity
K	Discharge loss coefficient
K_l	Light extinction coefficient
K_m	Mass extinction coefficient
$\dot{m}$	Mass flow rate
N_{elev}	Number of elevator shafts
v	Kinematic viscosity
Nu	Nusselt Number
R	Gas constant
P	Pressure
ΔP	Pressure difference
Pr	Prandtl number
$\dot{Q}$	Heat transfer rate
ρ	Density
Re_D	Reynolds number
T	Temperature
T_w	Wall temperature
σ	Stefan Boltzmann constant
t	Time
χ_s	Soot yield
Y_{soot}	Soot mass fraction
Vis	Visibility
$\dot{\forall}$	Volumetric flow rate

Subscripts

atm	Atmosphere
b	Building
elev	Elevator
env	Building envelope
f	Floor
ff	Fire floor
HRR	Heat release rate
*L*1	1st floor
*L*17	17th floor
out	Outside
ovr	Overall
ref	Reference
sh	Elevator shaft
sw	Shaft wall
th	Theoretical
w	Wall

Abbreviations

CFD Computational fluid dynamics
ELA Effective leakage area
FDS Fire dynamics simulator
HVAC Heating ventilating and air conditioning

1. Introduction

Fire safety in high-rise buildings continues to receive attention because of the potential for significant loss of life [1, 2]. Improving fire safety in high-rise buildings requires better understanding of (1) flammability of high-rise building materials; (2) ignition and fire spread and growth; (3) smoke transport and control; (4) structural response and (5) human evacuation [3]. Effort is being made in developing improved structural fire protection models and standards as the structural stability of high-rise buildings during a fire event limits the overall hazardous impact. A more likely threat to inhabitants of high-rise buildings affected by fire is smoke spread. Occupant safety and egress is strongly dependent on smoke spread through occupant incapacitation and wayfinding [4, 5]. Fire generated smoke is comprised of incomplete products of combustion which can act as asphyxiants (e.g., CO and HCN) and irritants (e.g. acrolein, unburned hydrocarbons, and soot) [6]. Combinations of these chemicals have been shown to reduce walking speeds [4, 5]. Smoke spread also affects wayfinding as smoke impairs vision and limits the overall visibility required to identify signage and exits. Smoke transport in high-rise buildings primarily occurs through vertical chases such as stairways and elevator shafts. The thermal stratification created by the fire modifies any natural stack effect associated with temperature differences between the interior of the building and the ambient environmental temperature.

The stack effect, which is the buoyancy driven flow into and out of buildings, is important in high rise buildings. Density differences between the inside and outside of the building cause buoyancy forces to move gases across openings and leakage areas throughout a building. As noted, the elevator shafts and stairways are one of the main pathways for smoke to be transported through the building. In cold weather, air penetrates a warmer building from the lower levels and rises through it, causing the building to behave like a chimney. This chimney effect can cause the transport of hazardous materials during a fire scenario in a building. There are historical cases in which this has happened and resulted in casualties [7]. In order to better understand the smoke movement physics of the problem, the characteristics of heat and mass transfer in the shafts needs to be investigated.

There are two main approaches to quantitatively analyze the smoke movement in high-rise buildings which are computational fluid mechanics (CFD) methods and network models. CFD methods numerically solve the Navier–Stokes equations and details of the flow throughout an area of interest. Network models are based on numerically solving coupled fundamental conservation equations of different zones within the region of interest. These zones are usually lumped repre-

sentation of rooms or shafts. Although CFD tools can provide information about spatial details of the flow, solving reacting flows in large domains like high-rise buildings can be computationally expensive. Therefore, simplified network models are still favorable due to their very fast prediction times.

Early studies of network models for smoke movement have been done by several authors [8–24]. Klote developed fundamental network and zone model approaches for analysis of the stack effect in building fires [9]. Walton developed a well-known network model, CONTAM which is frequently used for air quality and ventilation analysis of buildings [10]. It can also be used for design of smoke management systems. Recent work on CONTAM has been conducted to add heat transfer to the model for high-rise fire smoke modeling [11]. Black developed a solver called COSMO which specifically solves the fundamental equations of smoke movement in elevator shafts in a high-rise fire [12]. The major differences between COSMO and CONTAM are that it includes heat transfer and solves the conservation of momentum equation in the shafts' control volumes. COSMO's limitation is that it is limited to steady state. A new version of COSMO uses a fire's heat release rate (HRR) instead of the fire temperature [13, 14]. COSMO has been used to design fire safety plans for different types of stairwell pressurization and ventilation configurations [15]. COSMO has been extended to be capable of modeling two types of shafts (elevator shafts and stairwells), which can also be pressurized [16–18]. Qi et al. solved the coupled heat and mass transfer equations of the elevator shaft to locate the neutral plane and estimate smoke movement in the shaft. Analytical estimations were compared with the results obtained from a CONTAM network solution [11, 19–21]. Qi et al. recently proposed a new Froude-Stanton model for heat and mass transfer in large vertical shafts of high-rise buildings. They verified the model by comparing with the experimental data that it was an improvement over Froude modeling in which temperature change in the shaft was not considered. It was mentioned that the new model is limited to steady state analysis, but can be extended to provide transient solutions [22].

Zhang et al. proposed a two-zone model to estimate the location of neutral plane in the shaft of a high-rise building in case of a fire. The results of the analytical model were compared with results using Klote's model and CFD results. However, their analytical model used the temperatures found from a CFD simulation, which could require a relatively expensive CFD calculation for each model prediction [23]. Zhang et al. developed a simplified steady state two zone model to predict the smoke movement in vertical shafts during a fire. They compared their results with the open source CFD code Fire Dynamics Simulator (FDS) and experimental data using a lab-scale shaft [24]. Bae et al. developed another steady state network-based smoke control program and investigated a first-floor fire scenario in an ultra-high-rise building and compared the results with the ones from CONTAM. Although the results were in good agreement, heat release rate was steady in their model and a particular fire temperature had to be used as an input to the model [25]. Chen developed a model to estimate vertical temperature distributions in ventilation shafts. They found good agreement with the experimental data obtained from a lab-scale shaft, however the velocity was assumed to be con-

stant in the shaft, which could be valid for lab-scale shaft geometries but is not a realistic assumption for high-rise buildings [26].

In addition to network models, there are several computational and experimental studies examining the stack effect with or without fires in high-rise buildings. Hadjisophocleous and Jia [27] performed a CFD simulation for a 2nd floor fire scenario in 10-story building with no elevator shaft. They compared their results with the experimental data and good agreement was found. Acikyol et al. [28] conducted experiments in a 40-story high office building in Istanbul to better understand the effect of a fire protection lobby, which is a small enclosed space between the corridor and the stairwell. It was found that the presence of the fire protection lobby increased the pressure difference between the stairwell and corridor by a factor of 2.2. This change minimized smoke transport to upper layers. Strege et al. [29] studied the stack effect within stairwells and elevator shafts by measuring differential pressures in 15 high-rise buildings in four different cities. The results of this study are used as experimental validation case in our study.

In this study, a transient network model is developed, and the results are compared with the ones obtained from the CFD tool, Fire Dynamics Simulator (FDS) [30]. Firstly, experimental validation was performed by modeling the non-fire stack effect case(s) detailed by Strege and Ferreira [29]. Then, a fire is placed at the first floor of a 17-story high rise building and a simulation is performed for a fire time of about 17 min (1000 s) for four different cases which are combinations of warm/cold ambient temperatures and loose/tight envelope tightness. Pressure and total mass on the fire floor are compared, and reasonable matches are found. Pressure, temperature and mass flow rate distributions in the elevator shaft are reported. Finally, smoke transport and visibility case studies are performed using the model.

2. Simplified Transient Network Model

The network model is based on defining zonal elements within a building solving a set of coupled conservation equations. In our formulation, each floor is comprised of two zones (an elevator shaft zone and a main/open floor space zone). Different floors are only connected via elevator shafts, which provides flow through elevator doors under the effect of a pressure gradient. The gas mixture on the fire floor is assumed to obey the ideal gas equation of state. As such, as the fire burns, the temperature and pressure increase, which drives flow into the elevator shaft. The elevator shaft is divided into equal volumes at each floor level, and conservation of mass and energy equations are solved for each volume. A schematic of the building showing the flow pathways and control volume of the fire room is presented in Fig. 1.

The underlying assumptions of the simplified model are summarized below

- All gases are modeled as air and assumed to be ideal.
- A simple radiative transfer model is applied between the fire and the walls through the use of a radiative transfer coefficient, h_r.

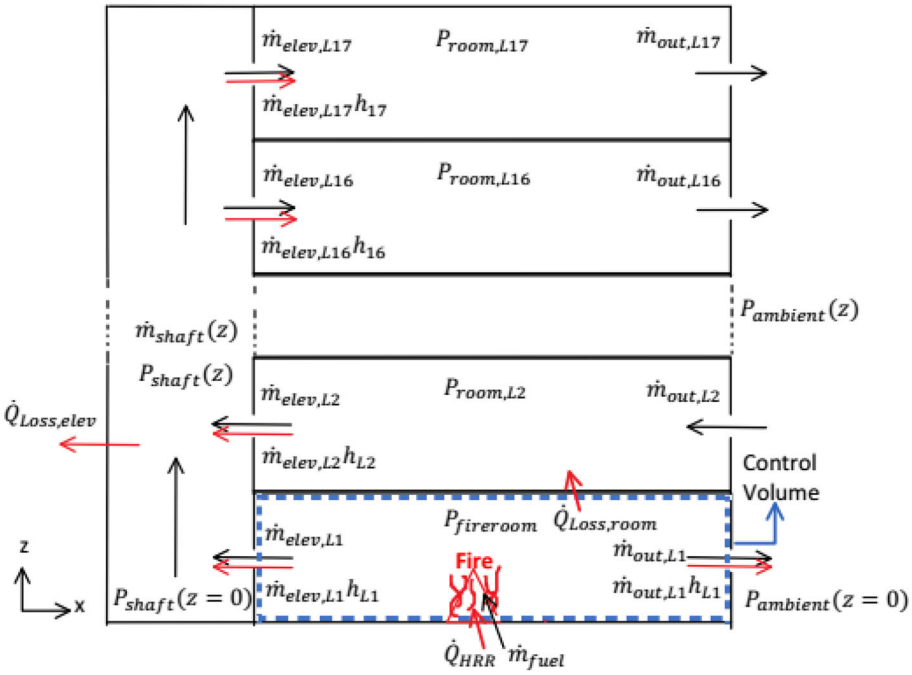

Figure 1. A schematic of the simplified model representing the flow pathways and the control volume of the fire floor.

- Interior walls are assumed to have constant temperature, $T_w = 20\,^{\circ}\mathrm{C}$.
- There is no external wind load on the building.
- The fire heat release rate is characterized using a t^2-fire model. The combustion is assumed to be fuel limited with $\dot{m}_{fuel} = \dot{Q}_{\mathrm{HRR}}/\Delta h_c$.
- The vertical pressure variation is based on a hydrostatic pressure computed using the instantaneous mean temperature.
- Flow is incompressible everywhere, but the density varies at the fire floor and the elevator shaft.
- Density is constant in elevator shaft and calculated based on ground level shaft pressure and mean temperature of the shaft at the previous time step.
- There are no stairwells in the building
- There are no elevator cars in the elevator shafts
- There is no momentum loss in the shaft due to friction
- There are no interior rooms or doors that might add additional flow resistance between the shaft and the outside.
- Flow resistances of the building envelope are identical at each floor and based on the building tightness in case of close windows and doors.

Conservation equations for the building system are detailed in the following sections. For the elevator shaft and the floors, pressure, temperature, mass flow rates, soot concentration and visibilities are solved by using the Eqs. (1)–(20).

2.1. Conservation Equations in the Fire Room

Conservation of mass for the fire compartment can be written as

$$\frac{\mathrm{d}m}{\mathrm{d}t} = \dot{m}_{fuel} - \dot{m}_{out} - \dot{m}_{elev} \tag{1}$$

The fuel mass flow rate, $\dot{m}_{fuel}$, is always positive, $\dot{m}_{out}$ is the mass transfer rate via the exterior walls and $\dot{m}_{elev}$ is the mass transfer rate via the elevator shaft doors. The parameters in the Eq. (1) are defined as

$$\dot{m}_{fuel} = \frac{\dot{Q}_{HRR}}{\Delta h_c} \tag{2}$$

$$\dot{m}_{out} = (C_d A)_{wall} \sqrt{2\rho \left| P - P_{out,z=0} \right|} sgn\left(P - P_{out,z=0}\right) \tag{3}$$

$$\dot{m}_{elev} = N_{elev} (C_d A)_{elev} \sqrt{2\rho \left| P - P_{sh,z=0} \right|} sgn\left(P - P_{sh,z=0}\right) \tag{4}$$

Knowing the ambient pressure distribution and the flow resistances at each floor, $P_{sh,z=0}$ is adjusted such that the continuity is satisfied in the elevator shaft. The conservation equations solved for the elevator shafts are explained in the next section.

For fire in a compartment, the energy equation is given in Quintiere as [31]

$$c_p \frac{\mathrm{d}}{\mathrm{d}t}(mT) - \forall \frac{\mathrm{d}P}{\mathrm{d}t} + \sum_{j,netout} m_j c_p T_j = \dot{Q}_{HRR} - \dot{Q}_{Loss} \tag{5}$$

The time derivative of the equation of state for an ideal gas is

$$\forall \frac{\mathrm{d}P}{\mathrm{d}t} = R \frac{\mathrm{d}}{\mathrm{d}t}(mT) \tag{6}$$

Implementing Eq. (6) to the energy equation (Eq. (5)) yields

$$mc_v \frac{dT}{dt} = \dot{Q}_{HRR} - \dot{Q}_{Loss} - c_v T \frac{dm}{dt} - c_p T \sum_{j,netout} m_j \tag{7}$$

Then, the coupled set of ordinary differential equations, (Eqs. (1) and (7)) can be solved simultaneously by using a Runge–Kutta method.

A simple Newton's law of cooling-based heat loss model is applied to the fire room.

$$\dot{Q}_{Loss} = h_t A_w (T - T_w) \tag{8}$$

h_t is the overall heat transfer coefficient, A_w is the total wall area at the fire floor and T_w is the wall temperature. The overall heat transfer coefficient consists of radiative and convective coefficients. ($h_t = h_c + h_r$)

Assuming turbulent natural convection in compartment fires, the convection heat transfer coefficient can be calculated from the following Nusselt number correlation given by Quintiere [31],

$$Nu = \frac{h_c H}{k} = 0.13 \left[\left(\frac{g(T - T_w)H^3}{Tv^2} \right) Pr \right]^{1/3} \tag{9}$$

where H is the height of the room and the others are the thermophysical properties of the air.

The radiative heat transfer coefficient can be estimated as [31].

$$h_r = \sigma \left(T^2 + T_w^2\right)(T + T_w) \tag{10}$$

Throughout the simulations with fire, h_r varied between 6 and 8 W/m^{2}K and h_c was approximately 5 W/m^{2}K.

2.1.1. Fire Model In many tall buildings, lobby or waiting areas consist of flammable decorations and furniture. In this paper, a first-floor fire is investigated. The fuel load is assumed to be polyurethane. Fire growth is modeled with a t-squared fire growth model [30] where the size of the fire is set using $\dot{Q}_{HRR,max} = 7.0MW$ based on a full scale fire test of a single office workstation by NIST [32]. The heat release rate can be written as [33].

$$\dot{Q}_{HRR} = \min\left(\alpha_f t^2, \dot{Q}_{HRR,max}\right) \tag{11}$$

Here $\dot{Q}_{HRR}$ is the transient fire heat release rate (HRR), α_f is the fire growth rate in units of kw/s^2, and t is the time from ignition. According to NFPA 204 M (National Fire Protection Association 1995) [34], the fast fire growth rate of $\alpha_f = 0.0469\,\mathrm{kW/s^2}$ is suitable for this scenario. Thus, the calculated duration of the fire

growth phase is 386 s. Note that the fire model in its current implementation does not simulate under-ventilated fire scenarios. It is assumed that the available oxygen within the lower level of the building and mass flow rate into the fire compartment provided by Eq. 1 provide a sufficient amount of oxygen to sustain the fire.

2.2. *Conservation Equations in the Elevator Shaft*

As previously noted, the elevator shaft is divided into equal control volumes such that there is one cell at each floor. Steady state conservation equations are applied. The pressure, temperature and mass flow rates in the shaft vary due to the changes of pressure and temperature at the fire floor.

Assuming incompressible flow in the shaft, conservation of mass states that the sum of mass flow rates from floors to the elevator should be zero.

$$\sum_i \dot{m}_{elev,i} = 0 \tag{12}$$

where the index i indicates the ith floor. The mass flow rate at each floor, except the fire floor, is determined by considering pressure differences between the elevator shaft and the building exterior and the associated flow resistances. Therefore, pressure in the elevator shaft and ambient at each floor level and associated flow resistances connecting them should be carefully determined.

The uniform density assumption through the elevator shaft implies that the pressure decreases with increasing elevation as:

$$P_{sh}(z) = P_{sh,z=0} - \rho_{sh} g z \tag{13}$$

Similarly, the pressure distribution exterior to the building can be written as

$$P_{out}(z) = P_{out,z=0} - \rho_{out} g z \tag{14}$$

where $P_{out,z=0}$ is the ambient pressure at the ground level, ρ_{out} is the ambient air density.

In each time step, the density of the elevator shaft is calculated by

$$\rho_{sh} = \frac{P_{sh,z=0}}{R T_{mean}} \tag{15}$$

where T_{mean} is the mean temperature of the shaft at the current time, which is calculated from the solution of temperature distribution in the shaft.

Theoretically, pressure difference between elevator shaft and the ambient due to temperature stratification can be calculated as in Eq. (16) [30].

$$\Delta P_{th}(z) = P_b(z) - P_{out}(z) = \left(P_{sh,z=0} - P_{out,z=0}\right) + (\rho_{out} - \rho_{sh}) g z \tag{16}$$

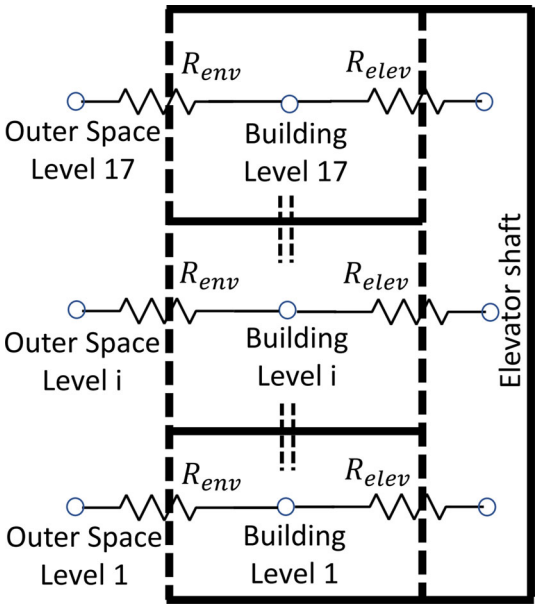

Figure 2. Flow resistances in the building.

The flow pathway between the exterior and the elevator shaft is depicted by a circuit analogy in Fig. 2. Please note that flow resistances are the same at each level.

Flow resistances through the elevator doors and the exterior walls are calculated as

$$R_{env} = \frac{1}{(C_d A)_{env}^2} \tag{17}$$

$$R_{elev} = \frac{1}{(N_{elev} C_d A)_{elev}^2} \tag{18}$$

The overall flow resistance for each floor can be calculated as

$$R_{ovr} = R_{env} + R_{elev} = \frac{1}{(C_d A)_{ovr}^2} \tag{19}$$

Once $(C_d A)_{ovr}$ is calculated, the mass entrainment rate to the shaft at each floor can be calculated as

$$\dot{m}_{elev,i} = (C_d A)_{ovr} \sqrt{2\rho |\mathrm{P_{sh,i}} - P_{out,i}|} sgn(\mathrm{P_{sh,i}} - P_{out,i}) \tag{20}$$

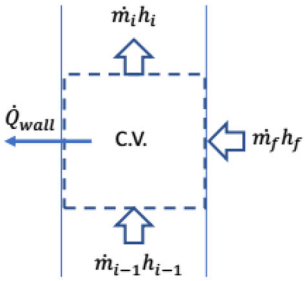

Figure 3. Schematic of a shaft cell control volume for energy balance in the elevator shaft for each floor.

Depending on the pressure difference between the shaft and the exterior, $\dot{m}_{elev,i}$ becomes positive or negative with certain modification in the code. Please take note that this equation is not used for fire floor, the model of which is described in previous section.

The temperature distribution inside the shaft is calculated by assuming ideal mixing of the entrained air with heat loss to the wall. A schematic of a cell control volume is shown in Fig. 3.

By writing the energy balance equations for all cells, a set of equations can be constructed. Then, unknown temperatures at each cell can be easily solved by any linear system of equation solver.

2.3. Determination of Flow Resistances

Flow resistances must be specified since they affect the flow characteristics in the building. Recall the leakage model

$$\dot{m} = C_d A \sqrt{2\rho \Delta P} \tag{21}$$

In this section selection of the leakage area A and discharge coefficient $C_d$for elevator door and building envelope will be discussed.

2.3.1. Elevator Door Flow Resistance An area survey of an actual elevator is done by He et al. [35]. The dimension of the elevator door is 1.07 m (42 inches) by 2.14 m (84 inches). Gaps are along the edges and the centerline of the door. The width of the gaps is approximately 4.76 mm (3/16 inch), which is equivalent to a total leakage area of 0.041 m^2 which is very close to 0.047 m^2 given by Klote. As a conservative consideration, 0.05 m^2 is used for a single elevator door. In the ASHRAE handbook [36] experimental investigations of the leakage rates for elevator and stair doors for a pressure difference of 70 Pa are presented. Using that data, discharge coefficient of 0.53 is calculated. [35], which corresponds to a loss coefficient of $K = 3.56$. based on the following relation

$$K = \frac{1}{C_d^2} \tag{22}$$

2.3.2. Building Envelope Flow Resistance Leakage through building envelopes have been extensively studied. The typical approach to the problem is measuring leakage rates under pressurization. In general, leakage data correlations are derived from building measurements based upon building features such as age, construction type, materials used, type of occupancy, etc. However, few data sets are available for high rise buildings.

In general, pressurization test results can be applied to orifice equation to determine leakage area, which can be normalized by using total wall area to generalize. The orifice equation is given as

$$\dot{\forall} = C_d A \sqrt{\frac{2\Delta P_{ref}}{\rho}} \tag{23}$$

The reference pressure (ΔP_{ref}) for leakage measurement tests can be performed using either 4, 10, 25, 50 or 75 Pa. In the ASHRAE handbook [36], the recommended pressures are 4 Pa and 10 Pa since they are closer to the actual pressure differences for leakage cases. It is also stated that some studies use a discharge coefficient of C = 0.65 and others use a parameter called the effective leakage area (ELA) by assuming a discharge coefficient of C = 1.0 at 4 Pa reference pressure. Using the definition of ELA, the orifice equation becomes,

$$\dot{\forall}_4 = ELA \sqrt{\frac{8}{\rho}} \tag{24}$$

where $\dot{\forall}_4$ is the flow rate for $\Delta P = 4\,\text{Pa}$. Conversion can be made between the leakage data at different reference pressures by using the power-law equation.

$$\dot{\forall} = C\Delta P^n \tag{25}$$

C is the same for most of the flows, and the exponent, n is usually very close to 0.65.

Using that, the effective leakage area conversion can be shown to be

$$\frac{ELA_1}{ELA_2} = \left(\frac{\Delta P_1}{\Delta P_2}\right)^{n-0.5} \tag{26}$$

Based on an office building data set available, Emmerich and Persily [37] concluded that effective leakage area for buildings taller than 10 stories converged to 3.33 cm^2/m^2 at 10 Pa reference pressure, which corresponds to 2.90 cm^2/m^2 at

4 Pa. Jeong [38] conducted an experimental study on two office buildings having 3 stories and 5 stories and determined effective leakage areas between 0.28 cm^2/m^2 and 1.38 cm^2/m^2 at 10 Pa, which corresponds to 0.24–1.20 cm^2/m^2 at 4 Pa. Klote et al. [39]. provided flow areas of walls of commercial buildings based on the experimental results of Tamura and Shaw [38–40]. Leakage areas given by Klote are based on $C_d = 0.65$ at a reference pressure of 75 Pa for four different tightness conditions which are converted to *ELA* and presented in Table 1. All other experimental data that we accessed in the literature are also converted to ELA at 4 Pa reference pressure and summarized in Table 2.

2.4. Building Model and Parameters Related to FDS Simulation

The building model is based on the study of He et al. which has 17 stories and has dimensions of 43 m, 66 m and 68 m in x, y and z respectively [35]. Each floor has 4 m height. Elevator shafts are defined as rectangular ducts having dimensions of 1.5 m to 2.5 m. For the case with fire, 8 elevator shafts are used. Flow paths consist of the envelope leakage which consists of construction cracks, windows and doors, and gaps of elevator doors and elevator shafts. There is no open door or window via exterior wall or via elevator doors, which means the flow is through leakages only. There is also no closed door within the floors.

FDS numerically solves the Navier–Stokes equations using the Large Eddy Simulation (LES) model for turbulence. LES is based on filtering the small scales of eddies and modeling them instead of resolving them. This is a suitable approach especially for reactive flows since most of the turbulent kinetic energy is carried by large eddies. As the focus of this paper is not on the turbulent flow physics, we did not explore differences in predictions between the LES based model and other types of turbulent flow models. For the fire simulation, the literature suggests that the LES based methodology in FDS is valid. For the flows in the elevator shafts, comparisons are made to experimental data for pressure differences. The LES based FDS predictions are reasonable for these problems.

Leakage through cracks are handled by a coupled network HVAC solver embedded in FDS [28, 41]. A cubic mesh with a grid size of 0.5 m was used for

Table 1
Leakage Areas for Exterior Building Walls Provided by Klote et al. [39]

Construction element	Leakage	A_{leak} ([39–42]) (m^2/m^2)	ELA (at 4 Pa) (m^2/m^2)
Exterior building walls (includes construction cracks around windows and doors)	Tight	5.0×10^{-5}	2.09×10^{-5}
	Average	1.7×10^{-4}	7.11×10^{-5}
	Loose	3.5×10^{-4}	1.47×10^{-4}
	Very loose	1.2×10^{-3}	5.02×10^{-4}

Data is based on Tamura and Shaw [40–42]) and calculated effective leakage areas (ELA)

Table 2
Experimental Data Available in Literature Converted to Effective Leakage Area (ELA) Based on 4 Pa Reference Pressure

Reference	ELA at 4 Pa (cm^2/m^2)
Klote [39] (based on Tamura and Shaw [40–42]	0.21, 0.71, 1.47, 5.02
Jeong [38]	0.24–1.20
Emmerich and Persily [37]	2.90

the FDS simulations reported in this study. There are two critical features of this problem that must be resolved: the fire the building flows. A characteristic fire diameter of 2.1 m is calculated using the scaling formula given in the FDS Technical Reference Guide [43]. It is recommended that the characteristic fire diameter to grid size ratio be between 4 and 12 to adequately resolve fires according to NUREG-1824 [44]. Therefore, the grid size of 0.5 m is within the range of sizes to coarsely resolve the fire. While this resolution is on the coarser side for the fire, it adequately resolves the relatively slow flows in the large building.

The walls have considerable thermal inertia that isolate the thermal effects on any given side over the time of interest in these calculations. The time required for heat transfer to reach the other side of any given wall can be defined using the thermal penetration depth. For concrete, the thermal diffusivity is $\alpha = 6.92 \times 10^{-7}$ m^2/s according to properties given in the literature [45]. For a wall thickness of 0.3 m, the time required for the inner surface to feel thermal changes on the opposite side is very large compared to the simulation times used in this project. Therefore, the walls are expected to behave like a semi-infinite medium for the simulation time of interest, which is $t = 1000$ s.

The overall computational cost will be very expensive when high rise building is analyzed, therefore the detailed heat transfer calculation within the walls is not computed. Instead, all walls are set to a constant temperature (i.e., the initial temperature of the interior) that is 20°C. Fire is defined on the floor of office area (ground level, z = 0 m) and specifically in $4\,\text{m} < x < 8\,\text{m}$ and $20\,\text{m} < y < 23\,\text{m}$ in FDS.

3. Results and Discussion

3.1. Experimental Validation (Case with no Fire)

Strege and Ferreira [29] experimentally measured the stack effect for 15 high rise buildings. They reported the pressure differences between the inside and outside of the buildings at the ground level and upper levels of the buildings. They also measured the pressure differences between the building and the elevator shaft through the doors connecting them. Two buildings from their data located in Minneapolis were selected as a benchmark for validation due to the similarity of the building heights with the building used in this study. The elevator door width is given as

Table 3
Specifications of Selected Buildings from Strege and Ferreira [29] Compared with the FDS Validation Model

Building#	Height (m)	Floors	Number of elevator hoistways	Number of stairwells	Outside temp (°C)	Inside temp (°C)
Exp [29]	69	19	4	2	− 8	23
FDS (6 shaft)	68	17	6	–	− 8	22
Our model	69	17	6	–	− 8	23

Building numbers are same as it is in the reference

1.2 m which is 3.5ft = 1.07 m in our case. The elevator door leakage area is set to 0.0483 m^2 in the model, which is provided in the experimental study. The perimeter of the building was found by using measurement tool of Google Earth as 190 m. The building contains 4 elevator shafts and 2 stairwells. Specifications of the selected buildings are provided and compared with our simulated model in Table 3.

The building model of this study was changed to be able to validate our model against their data. Such that: a door is located at the ground level, the number of elevator hoistways are selected as 6, elevator door leakage area is changed as 0.04831 m^2 and the no fire scenario is considered. A loose leakage scenario is defined for exterior doors.

Ground level and upper level pressure differences are compared in Table 4. $P_{sh} - P_{out}$ is dominated by shaft to ambient temperature difference. However, pressure differences through the elevator doors and exterior walls depend on the corresponding leakage resistances. Adding stairwells is very similar to increasing the number of elevator hoistways, so that a 6 elevator shafts are used in our model instead of 4 to include the effect of stairwells.

In both the network and FDS models, using a loose envelope tightness at each floor resulted pressure differences at the ground level that are close to the experimentally measured ones; the percent differences are no more than 20% between the exterior and the building interior zone and 30% between the interior building zone and the elevator shaft zone. However, pressure differences are overestimated at upper levels with approximately 90% error. Using identical tightness for each floor led to pressure differences of similar magnitudes at the ground and upper levels, which is expected in theory but was not the case in the experimental results. The building is a hotel building and there is an open skybridge connecting this building to adjacent building and a revolving door at the entrance, which makes the first two levels looser than the upper levels. To examine this effect, some modifications are applied to our network model. First, the envelope tightness is set to an average tightness (the value in Table 1) for the levels between 3 and 17 while first two levels are kept loose. The height of the second level is set to 5 m while other levels have 4 m height. These modifications lead to a significant decrease in upper level pressure difference, and the percent error of at the upper level decreases to 32%. Additionally, the pressures at the ground level are also closer to the

Table 4
FDS Model Validation with Experimental Study of Strege and Ferreira [29]

Data source	Envelope tightness	$P_{b,L1} - P_{out,L1}$ (Pa)	% Diff. from exp	$P_{sh,L1} - P_{b,L1}$ (Pa)	% Diff. from exp	$P_{sh,L17} - P_{b,L17}$ (Pa)	% Diff. from exp
Exp [29]	–	− 24.9		− 12.0		8.7	
FDS	All loose	− 27.1	8.6	− 15.8	31.8	16.1	85.1
Our model	All loose	− 29.7	19.31	− 16.1	34.5	16.8	93.2
Our model	Average L3–L17 exterior	− 27	8.4	− 14.7	22.8	5.9	31.7
Our model	Average L3–L17 exterior + extra door at L17	− 27.6	10.92	− 15.1	25.75	10.8	24.4

experimental values (8% error via exterior, 20% error via elevator doors). There is a small additional story at the rooftop which may cause extra leakage at the upper level. An additional door pathway is defined at uppermost level to handle this which has the same resistance as the elevator door. This small addition raised the pressure difference at the upper level such that the percent error is further decreased to 24%.

Although the modifications discussed above are not fully representative of all architectural layout details of the building, it shows that our network model predicts the trends in the pressure distribution in the building. The experimental data were taken during the normal building activity. The presented pressure differences are dependent on the architectural layout of the building and operating conditions of HVAC and elevators. Architectural details of the building can be easily implemented to the network model by changing the flow resistances and can be calibrated using any existing data because of the extremely fast run time of the code compared to CFD simulations.

3.2. First Floor Fire Scenario

Four different cases are examined which consist of the combinations of cold and warm environments with tight and loose envelope tightness. These cases are tabulated in Table 5. 8 elevator shafts are used in all cases.

3.2.1. Fire Floor Pressure variations and discharge characteristics in the fire room are discussed in this section. The network solutions (with a subscript *th*) is compared with FDS solutions.

Table 5
Different Cases Considered for First Floor Fire Scenario

Case	T_{out} (°C)	ELA of exterior walls
Cold, loose	− 15	1.47×10^{-4}
Cold, tight	− 15	2.09×10^{-5}
Warm, loose	20	1.47×10^{-4}
Warm, tight	20	2.09×10^{-5}

In Fig. 4, pressure variations are presented. For all cases, pressure has a peak value at approximately 400 s. It is nearly independent of ambient temperature but increases significantly when the building envelope is tightened. The network solutions show reasonable agreement with the FDS solutions for the loose envelope simulations. There is more error in the tight envelope simulations. For the tight envelop cases, there are errors in the time to peak pressure and the magnitude of peak pressure. The time shift between pressure curves is clearer in tighter cases than in looser cases. Moreover, the highest pressure is overestimated with the network model compared to the FDS predictions. Percent differences of highest gauge pressures of the network model compared to the results from FDS are given in Table 6. For loose cases, the differences are no more than 3%. However, the percent differences reach approximately 47% for tight cases. For the same level of envelope tightness, network pressure predictions for warm cases are more accurate compared to cold case predictions.

The elevated pressure on the fire floor causes mass flow to lower pressure zones. Characterizing the discharge behavior is critical to modeling the smoke transport. The total mass contained within the fire floor at the end of the simulation provides an estimate of much mass (smoke) had been discharged during the fire event. This serves as a useful parameter to use in validating the network model against FDS predictions.

In Fig. 5, the total mass of gas on the fire floor is plotted. The network model discharged the gases and reaches steady state slightly faster than FDS. The final total mass is overestimated in the network model which means that the total discharge amount is underestimated. The percent differences between the final total masses are given in Table 6 which vary between 1.68% and 8.15%. The spatial distribution of temperature within the fire floor is not considered in the network model. In reality, hot product gases accumulate near the ceiling and colder gases are near the floor. Because the elevator door gaps run from floor to ceiling, temperature of the gas entering the elevator shafts are different than the average temperature on the fire floor. Therefore, differences in the total discharge amount are observed between the network model and FDS, even when the pressures agree.

3.2.2. Elevator Shaft The problem of interest is characterized by a range of time scales. The shortest time scales are associated with turbulent eddy dynamics while the longest scales are associated with the fire growth times. The goal for FireSTORM is to predict transient effects on the fire time scales, and as such it is use-

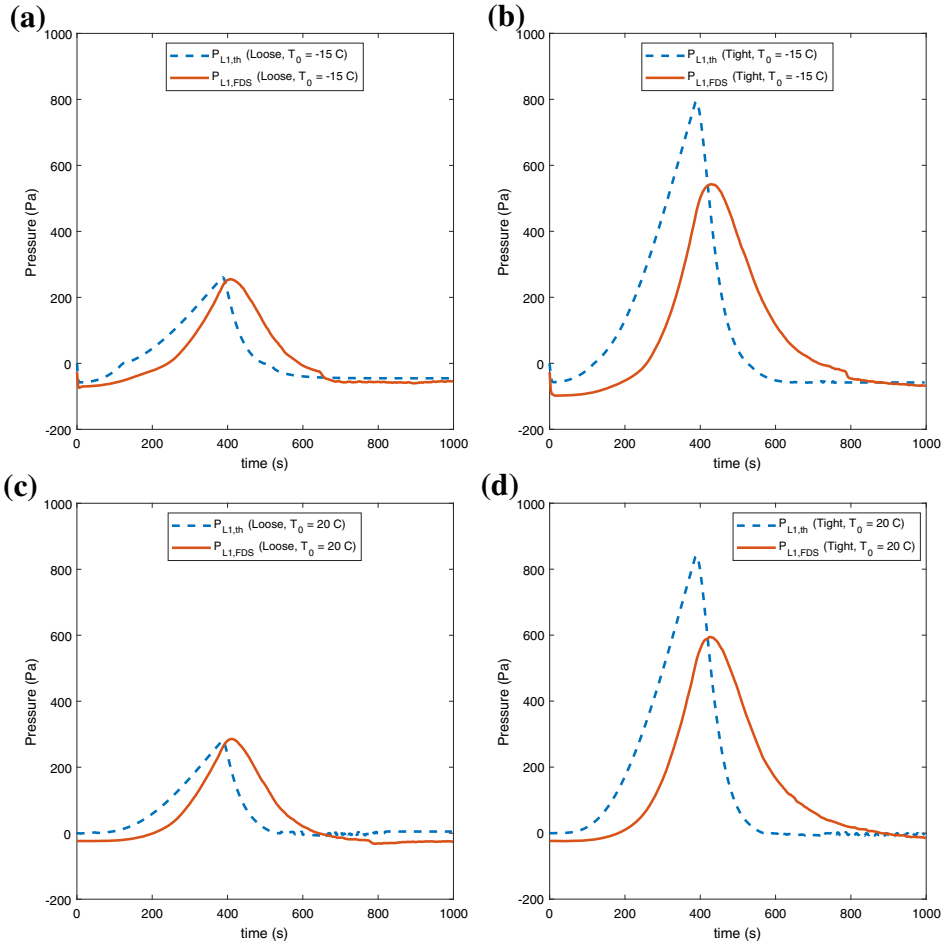

Figure 4. Time variation of gauge pressures in the fire floor (a) cold, loose (b) cold, tight, (c) warm, loose, (d) warm, tight.

Table 6
Percent Differences Between FDS and Our Model for Pressure and Total Mass at Fire Floor

Case	%Diff of max gauge pressures	%Diff of total mass at t = 1000 s
Cold and loose	2.67	7.08
Cold and tight	46.43	1.68
Warm and loose	1.50	8.15
Warm and tight	41.45	4.24

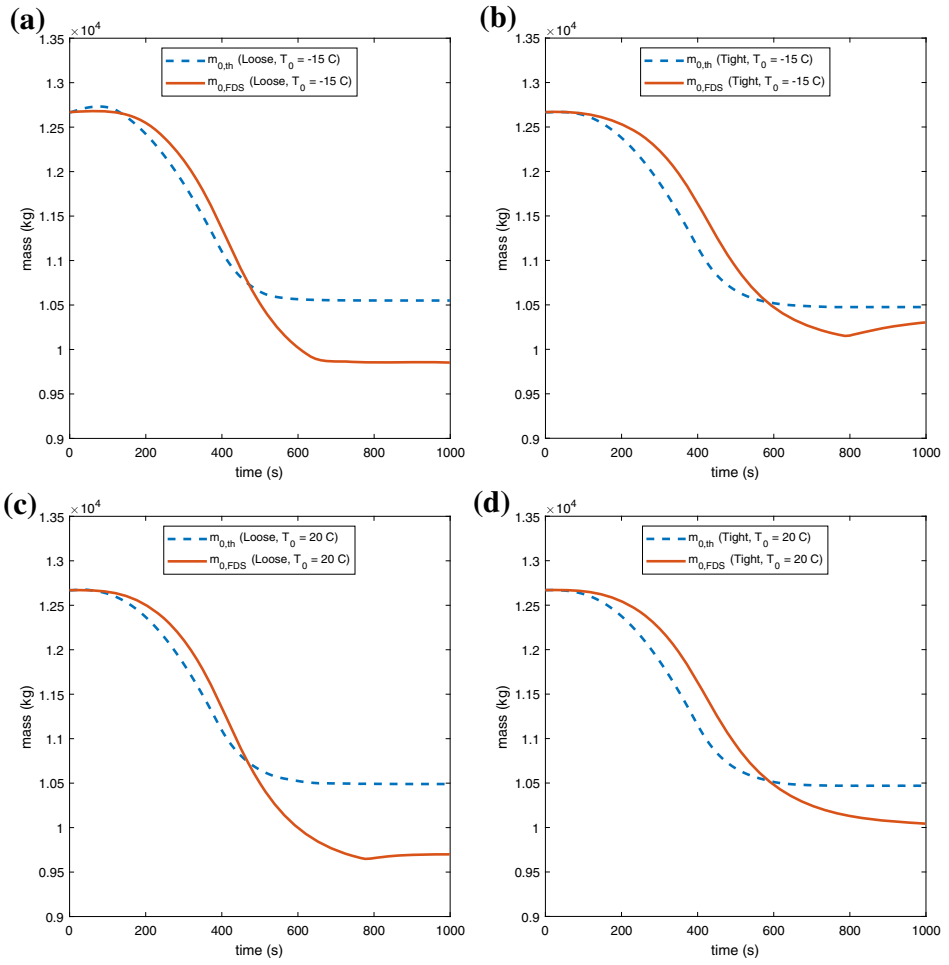

Figure 5. Time variation of total mass in the fire floor (a) cold, loose, (b) cold, tight, (c) warm, loose, (d) warm, tight.

ful to evaluate the effects of filtering FDS results when comparing with FireSTORM. As an example, the mass flow rate time history at 24 m height in the elevator shaft is presented in Fig. 6. In addition to the low-amplitude, higher frequency transients associated with eddies, there is a high-amplitude, low-frequency oscillation after 400 s for the tight envelope case. We believe that these low frequency oscillations are associated with transient density, pressure coupling in the shaft. The period of oscillation is approximately 100 s which is comparable to the characteristic time scale using the shaft length and a characteristic mean velocity in the shaft. Since the simplified model is incapable of resolving such a phenomenon, the data is smoothened by using Savitzky–Golay filter. Using a time-window of 20 s, first order fitting is applied on every data point. For the results

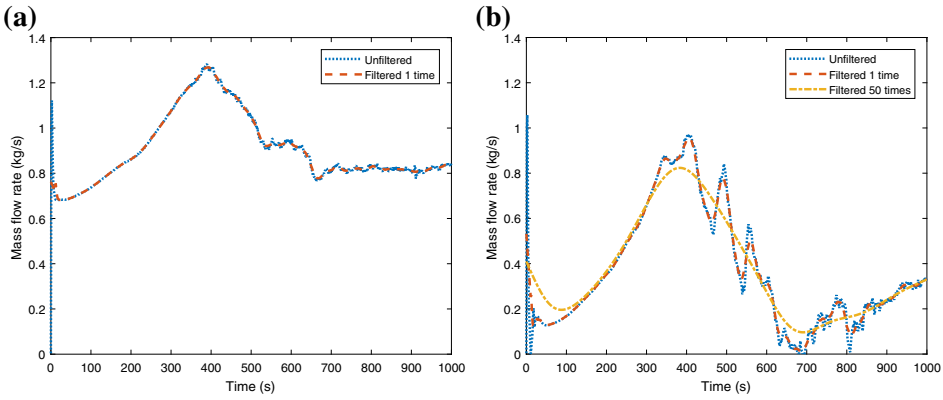

Figure 6. Time history of mass flow rate at 24 m height of elevator shaft (a) cold-loose, (b) cold-tight cases.

discussed in the following sections, the FDS data is filtered once for loose cases and 50 times for tight cases.

The mass flow rate distributions in the elevator shaft are given in Fig. 7. For all cases, the mass flow rates increase until the neutral plane and then decrease afterwards. The mass flow rates increase more at later times in the loose cases than in tight cases. The network model is in very good agreement with FDS for cold and loose cases and in reasonable agreement in warm loose and warm tight cases.

Pressure differences between the shaft and ambient are plotted in Fig. 8. The network model is in good agreement with FDS except at the early times for tight cases. As can be seen in Fig. 8b, d, there are considerable differences between the FDS and fire-STORM predicted pressures for the tight envelope cases. Looking at Fig. 4b, d, one also sees that there is a time offset of approximately 100 s in the time to peak pressure for the tight cases. To clarify the impact of a time-offset on the differences between the FDS and fire-STORM predictions, we shifted the fire-STORM pressure predictions by this 100 s offset and found closer agreement to the FDS predictions. There is likely an optimal but arbitrary time shift that would minimize the error. The existing error appears to be a fundamental limitation of the fire-STORM model for tight envelope simulations.

The location of the neutral plane is around half the height of the building for loose cases. The neutral plane moves downwards in tight cases and disappears at certain times due to pressurization of the shaft by the high pressure on the fire floor. The slope of the pressure differences is directly related to the temperature stratification differences between the elevator shaft and the environment. Therefore, the slopes are larger in cold cases than warm cases.

Accurate estimation of temperature in the shaft is very important since temperature differences drive the flow through the elevator shaft. Temperature distributions in the shaft are presented in Fig. 9. Similar to pressure and mass flow rate results, the network model most closely agrees with the FDS results in cold and loose cases. For all other cases, the network model overestimates the tempera-

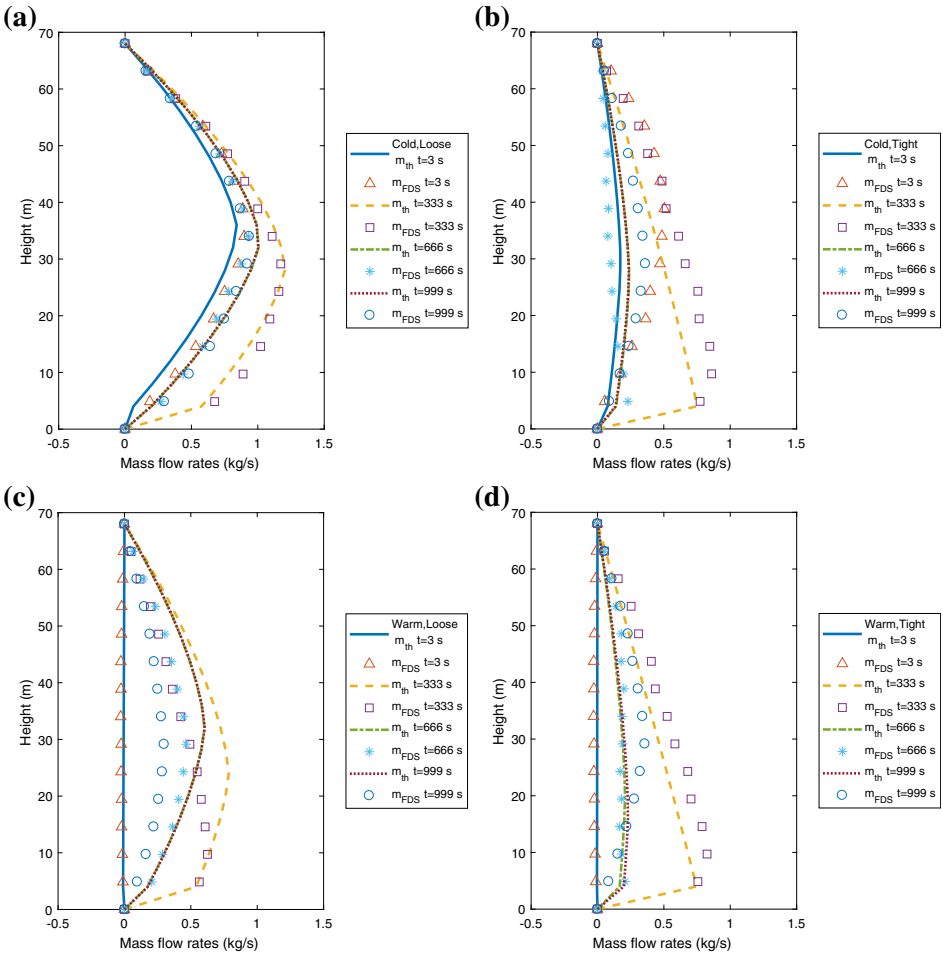

Figure 7. Time variation of mass flow rates in the elevator shaft (a) cold, loose, (b) cold, tight, (c) warm, loose, (d) warm, tight.

tures. While the heat loss model in the elevator shaft is reasonable for the network model, the temperatures at the inlet of the shaft are overestimated. This is because FDS predicts that the gases entering the elevator are colder than the average compartment temperature. Further, temperatures are unsteady in FDS while they are essentially steady by about 650 s in the network solution.

The mean temperature in the shaft determines the hydrostatic pressure distribution in the shaft. The network model estimates the mean temperature better in loose cases than in tight cases and in cold cases than warm cases.

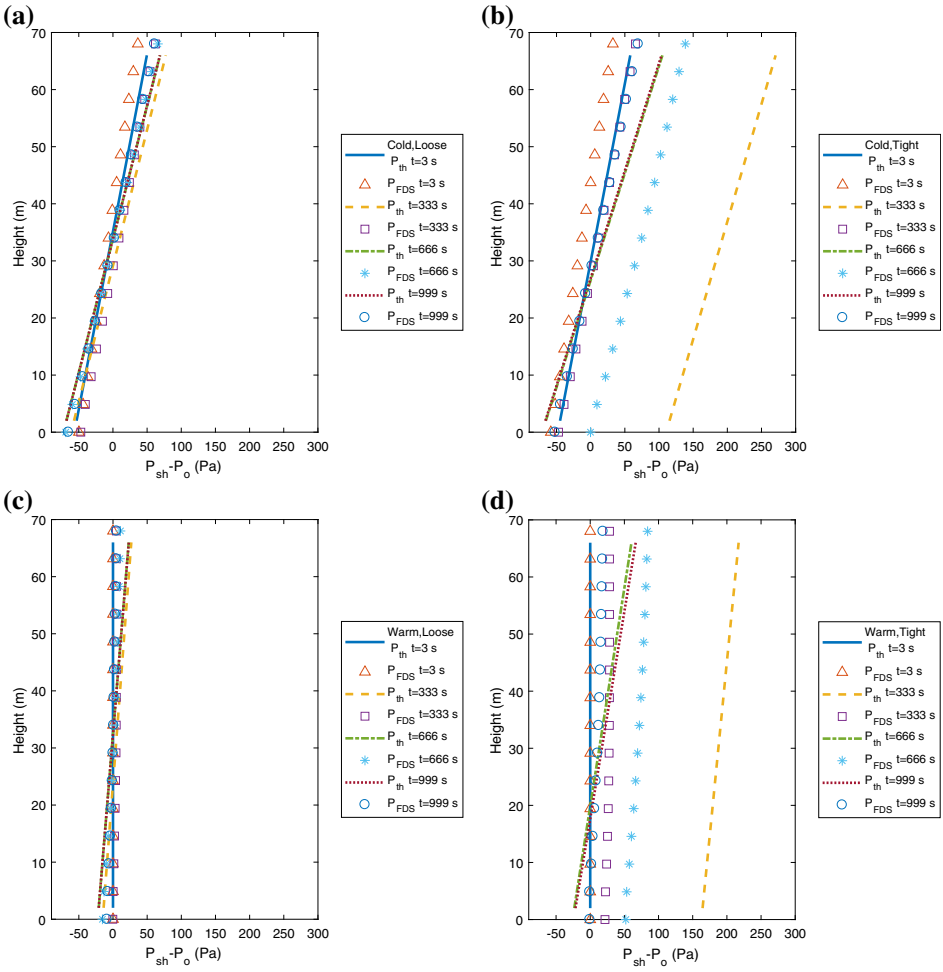

Figure 8. Time variation of pressures in the elevator shaft (a) cold, loose, (b) cold, tight, (c) warm, loose, (d) warm, tight.

4. Application

As an application, we consider the problem of smoke spread and visibility changes on the different floors of the building. One of the important design issues for tall buildings is the modeling of smoke transport. As previously noted, smoke influences occupant evacuation through visibility and signage issues and also from health, toxicity, and mobility perspectives. There are two main elements to performing such calculations. There is a need to construct accurate soot generation and transport models as well as a need to translate the soot volume fractions into measures of visibility and opacity.

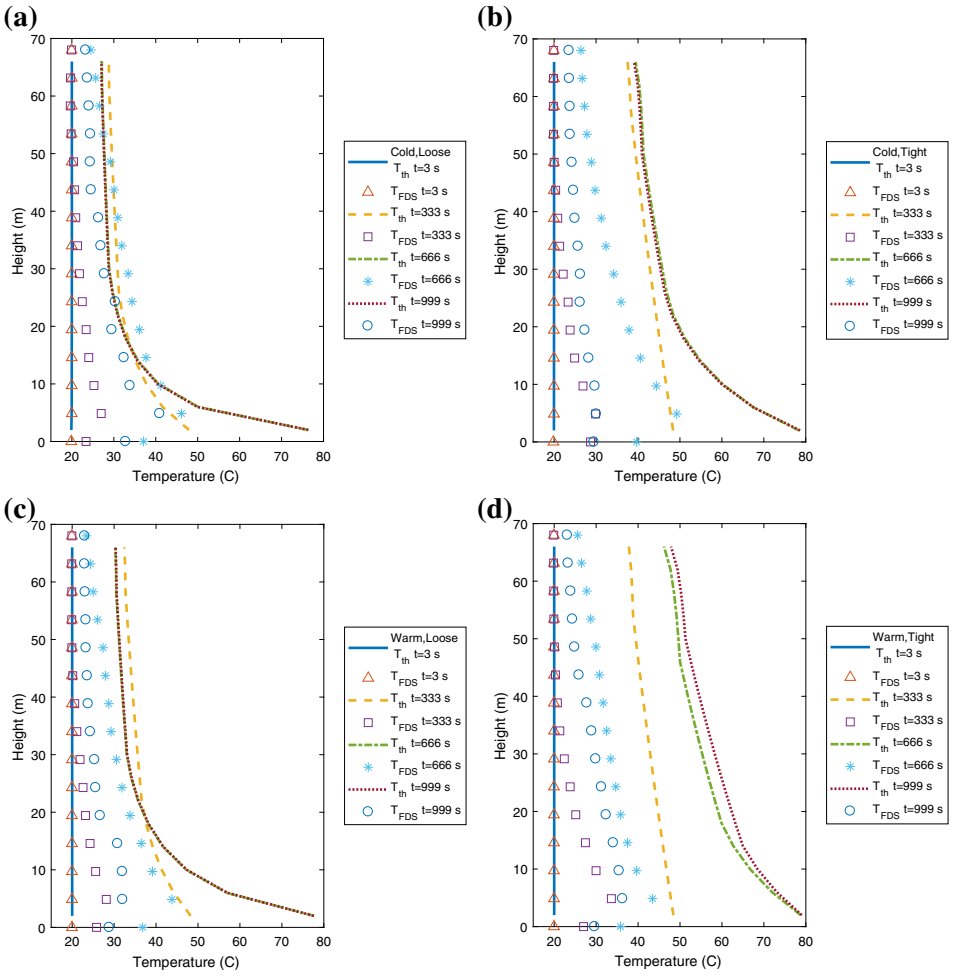

Figure 9. Time variation of temperatures in the elevator shaft (a) cold, loose, (b) cold, tight, (c) warm, loose, (d) warm, tight.

4.1. Theoretical Calculation of Soot Mass Fraction

Conservation of mass for soot can be written at the fire floor as

$$\frac{\mathrm{d}m_{soot,ff}}{\mathrm{d}t} = \dot{m}_{fuel}\chi_s - \dot{m}_{elev}Y_{soot,ff} - \dot{m}_{out}Y_{soot,ff} \tag{27}$$

The subscript, ff refers to fire floor in the Eq. (27). According to cone calorimeter tests conducted by Babrauskas, the amount of soot production per fuel consumption, known as the soot yield (χ_s), is approximately 0.1 for foam materials [46, 47].

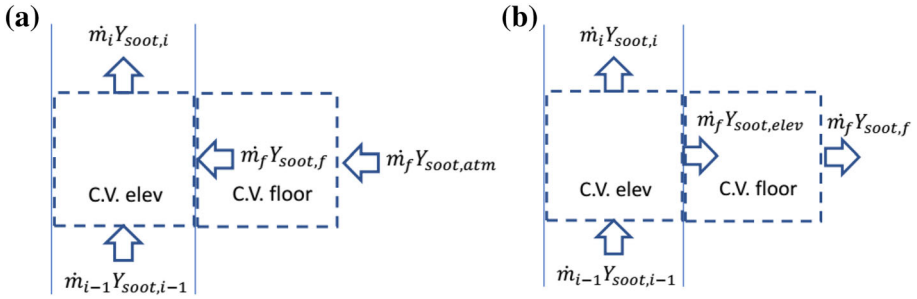

Figure 10. Schematic of control volumes for conservation of mass for soot at elevator partition and floor (a) flow is from the floor to the elevator, (b) flow is from the elevator to the floor.

Equation (27) is coupled with the mass and energy conservation equations of the fire floor and solved with them. Control volume balances for the soot mass fraction calculation are shown in Fig. 10.

In Fig. 11, soot mass fraction (Y_{soot}) in the elevator shaft is presented for different cases at different times. For all cases, the simplified theoretical model results are in good agreement with the FDS solutions, especially for the cold-loose case. For t = 333 s, the simplified model predicted soot everywhere in the shaft, whereas FDS predicts no soot at higher levels. Because the simplified model does not discretize the elevator space as finely as FDS does, the soot was immediately transmitted upwards in the simplified model. This causes Y_{soot} overestimations at the initial times while the elevator shaft zones are being filled with the soot. Moreover, Y_{soot} is underestimated for tight cases at upper levels due to discrepancies in mass flow rates.

In Fig. 12, the average soot mass fractions at different floors are presented for different cases. Results of the simplified theoretical model are in good agreement with the results of FDS. In the cold loose case, FDS predicted that soot exists at lower levels while the simplified model does not. In FDS, soot coming out from fire floor to the external environment rises along the outside wall by buoyancy forces and penetrates the lower floors with the flow from the outside via exterior leakage.

For both elevator shaft and floors, the external/ambient temperature does not affect the soot mass fraction significantly for the tight cases. Soot is transported to upper levels quickly in cold-loose cases compared to other cases.

4.2. Visibility Calculation

Visibility loss due to smoke is a potential hazard which inhibits the evacuation of people from the building. It can be assumed that light intensity decreases exponentially from its source with a light extinction coefficient, which can be written in terms of the mass specific extinction coefficient (K_m) and soot density as follows. [30]

$$I/I_0 = \exp(-K_m \rho Y_{soot} L) \tag{28}$$

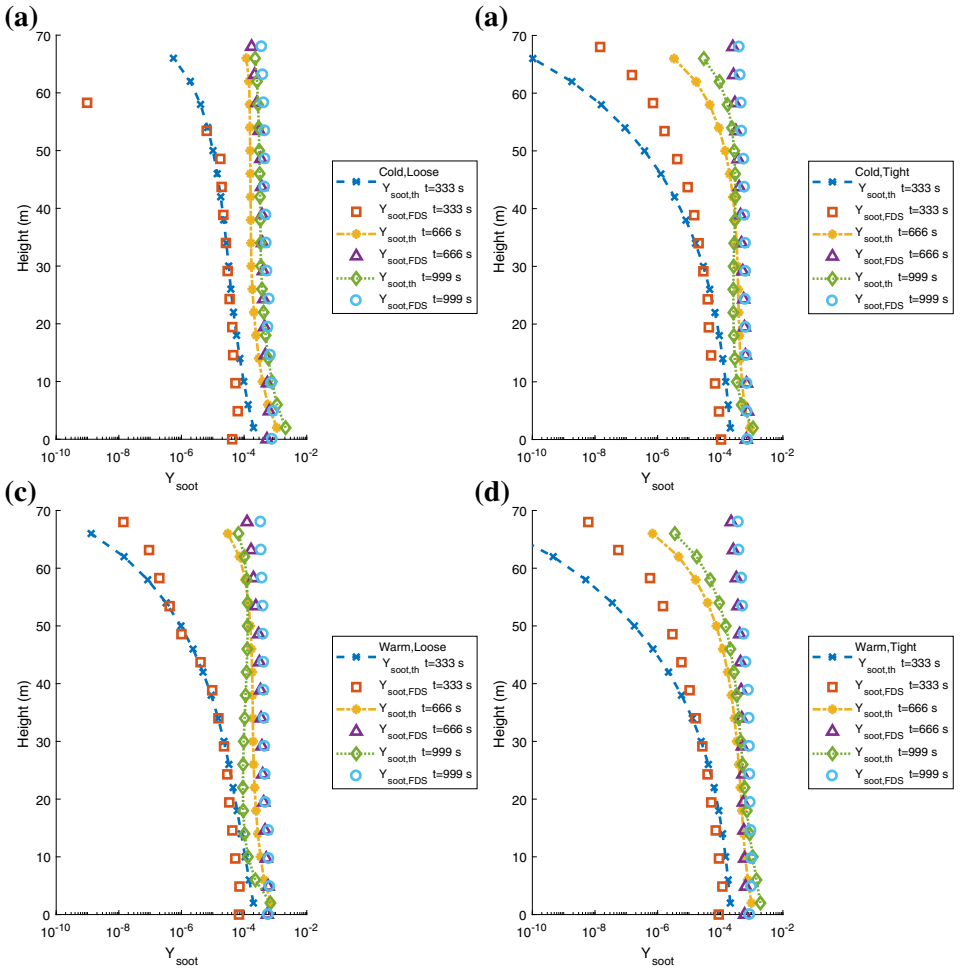

Figure 11. Soot mass fraction in the elevator shaft (a) cold, loose, (b) cold, tight, (c) warm, loose, (d) warm, tight.

Then, visibility can be defined as [30]

$$K_l = K_m \rho Y_{soot} \tag{29}$$

$$Vis = \frac{C}{K_l} \tag{30}$$

C is a nondimensional constant that depends on smoke and signage properties and ρ is the density of the fluid that contains soot. In our case, $K_m = 8700\,\mathrm{m}^2/\mathrm{kg}$ and $C = 3$ (suggested for reflected signage) are taken which are default values of

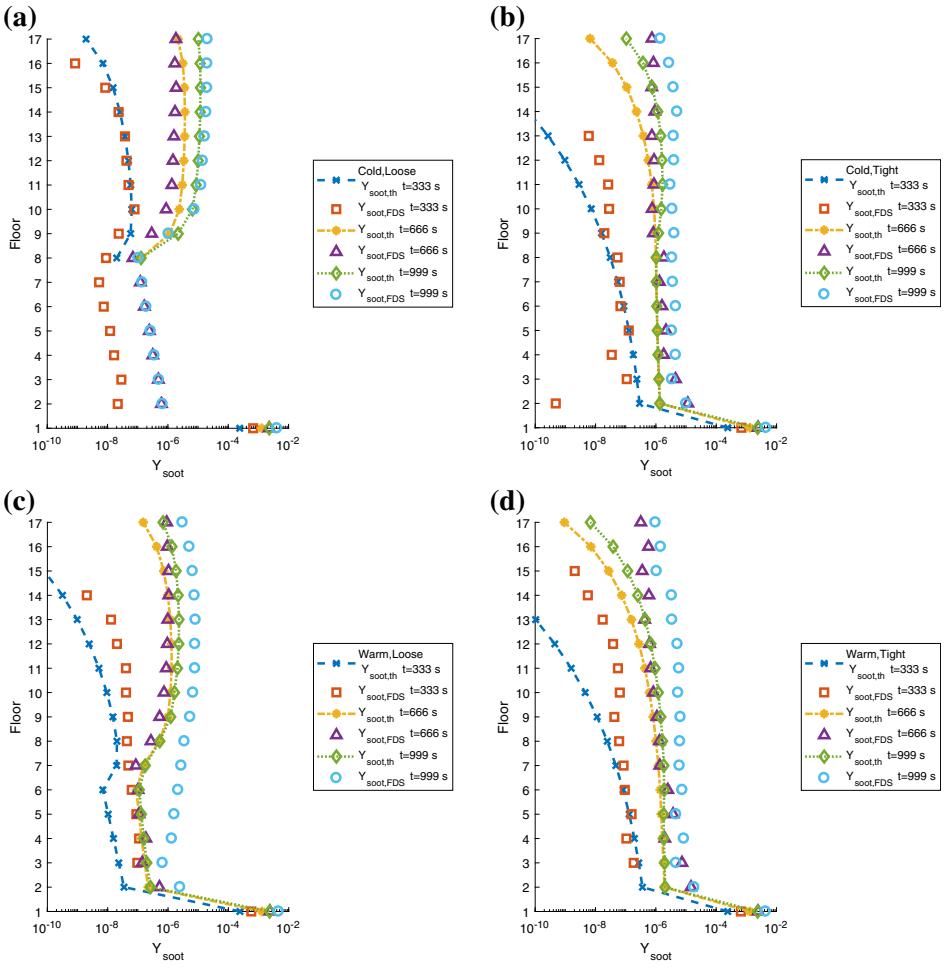

Figure 12. Soot mass fraction on floors for different envelope and ambient thermal scenarios (a) cold, loose, (b) cold, tight, (c) warm, loose, (d) warm, tight.

FDS [30]. Density is calculated by using the ideal gas law with calculated pressures and temperatures for the elevator shaft and fire floor, while it is taken as constant at other floors. ($\rho_f = 1.225\,\mathrm{kg/m^3}$, which is the density of air at 25°C and 1 atm [45]).

According to the visibility formula (Eq. (30)), as $Y_{soot} \rightarrow 0$ $Vis \rightarrow \infty$. To eliminate this, FDS sets a maximum visibility value of 30 m, which is reached when $Y_{soot} \cong 10^{-5}$. For this reason, all visibilities presented in this paper are 30 m if Y_{soot} is approximately 10^{-5}.

Visibility in the elevator shaft and average visibility on the floors are presented in Figs. 13 and 14 respectively. Since visibilities are inversely proportional to soot

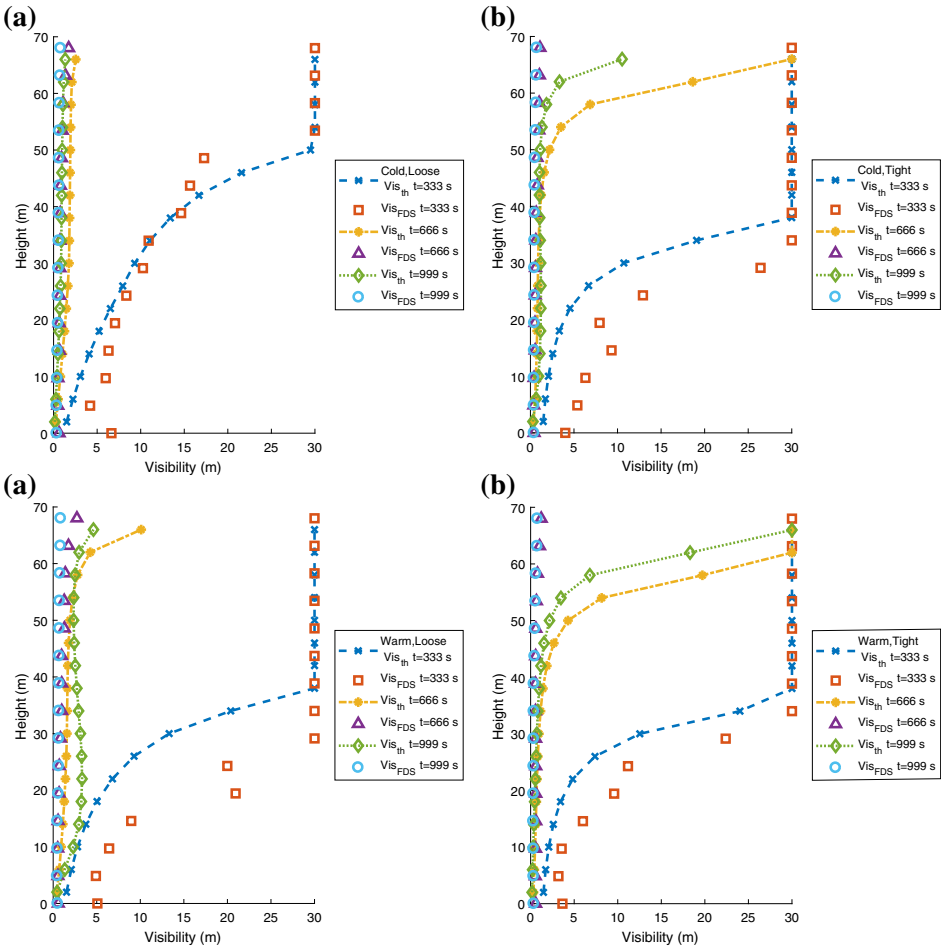

Figure 13. Visibility in the elevator shaft for different envelope and ambient thermal scenarios (a) cold, loose, (b) cold, tight, (c) warm, loose, (d) warm, tight.

mass fraction, similar discussions made for soot mass fraction can also be made for visibilities. Despite this similarity, visibility is considered as a metric that is easier to understand and visualize. It connects the science and mathematics with an easily understood parameter affecting evacuation metric. Different mass extinction coefficients could be addressed in the model, but we ultimately chose to keep it the same as the approach used in FDS. As expected, Fire-STORM and FDS results are in good agreement. However, visibilities are overestimated by the simplified model for tight cases at upper levels of the elevator shaft due to discrepancies in estimating the mass flow rates in the elevator shaft. Comparing cold-loose case with the others, it can be deduced that stack effect reduces the visibilities at uppermost levels quickly. Fire-STORM overestimated visibilities in tight cases compared to FDS results, which reminds that it should be used cautiously for

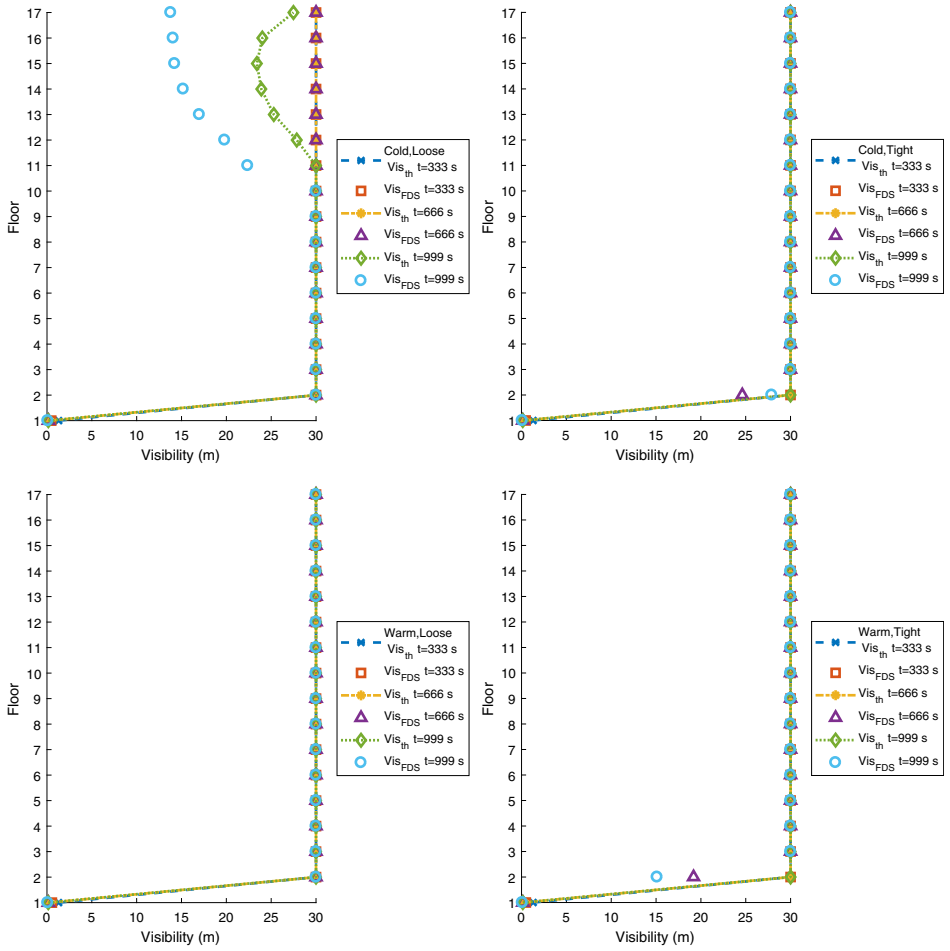

Figure 14. Average visibility on floors for different envelope and ambient thermal scenarios (a) cold, loose, (b) cold, tight, (c) warm, loose (d) warm, tight.

tight cases. Average visibilities at the floors other than fire floor are all 30 m except the cold-loose case, which indicates that discrepancies in small soot mass fractions do not affect visibility.

4.3. Simulation Times

Simulation times of the simplified model and FDS are compared in Table 7. The simplified model is extremely fast compared to FDS. All cases were solved in 30 s with the simplified model while FDS runs lasted about 1 week. In FDS, cold cases are slower compared to warm cases due to smaller time step requirement to satisfy

Table 7
Comparison of Simulation Times of Simplified Model and FDS for Different Cases

Case	Simplified model (s)	FDS (day:hour:min)
Cold, loose	25.9	7:20:21
Cold, tight	26.1	8:05:04
Warm, loose	26.7	5:00:28
Warm, tight	26.4	5:23:31

the Courant Friedrichs Lewy (CFL) stability constraint [43]. The somewhat increased flowrates for the cold cases require smaller time steps.

5. Conclusion

In this study, a transient network model (Fire-STORM) is developed, and results from it are compared against those from a CFD (FDS) tool. Fire-STORM solves a coupled set of differential equations for the fire floor in conjunction with conservation equations applied to the elevator shaft and other building zones. Fire-STORM quickly predicts the transient flow behavior in the shaft. In the non-fire experimental validation case with stack effects, a maximum error of 25.75% is obtained for pressure differences. The error is likely due to differences between the architectural details in the actual building that were not specified in the model description.

A first-floor fire scenario was investigated for a similar building structure with both Fire-STORM and FDS. Four cases which are combinations of ambient temperatures and envelope tightness were examined. The best agreement was achieved for a cold and loose case, because the flow in the elevator shaft is dominated by the stack effect which can be estimated very well using the network model. However, when there is less thermal/temperature stratification and the envelope is tight, more complex flow phenomena occurs in the building and the accuracy of the Fire-STORM decreases. An error of approximately 100 s occurs in the time to peak pressure on the fire floor for tight cases. Also, the maximum pressure on the fire floor is overestimated by Fire-STORM relative to FDS by approximately 45% for the tight envelope cases, which dramatically shifts the pressure in the elevator shaft and causes some inaccuracies in mass flow rates.

Temperature in the elevator shaft is usually overestimated with Fire-STORM. Good agreement is obtained when the mass flow rates in the shaft were high. Entrainment of cool air from floors above the fire floor into the elevator shaft reduced the gas temperature in the elevator shaft which minimized the effect of the initial temperature overestimations of the Fire-STORM model. The main reason for the elevator shaft temperature is the overestimation of temperature at the fire level of the elevator shaft. Fire-STORM assumes isothermal fire floor whereas

FDS fully resolves the temperature distribution. Air colder than the average temperature of the fire floor enters the elevator shafts in FDS since the elevator door gap spans the height of the floor and provides gas access to the shaft from the lowest and coolest parts of the ground level. Developing a 2-layer zone model for fire floor might decrease the deviations in temperature and mass flow rates between the network model and FDS.

Overall, the new network model (Fire-STORM) does a reasonably good job in predicting the flow parameters in the elevator shafts, especially when the envelope tightness is loose and stack effect is dominant. Despite its error for some cases, such simplified network models are promising due to the advantage of quick run times (seconds) over CFD models (days) which provides possibilities for performing thousands of analyses in very short times. Therefore, different buildings in various environment conditions can be analyzed for different fire scenarios to perform fire risk analysis and/or optimize the firefighting tactics. Integrated with smart sensor systems, such fast network codes can be used to predict and monitor the real-time changes of flow pathways in the building during the building activity or fire.Publisher's NoteSpringer Nature remains neutral with regard to jurisdictional claims in published maps and institutional affiliations.

Acknowledgements

This work was funded by the Federal Emergency Management Agency's Assistance to Fire-Fighters Grant Program under Grant EMW-2016-FP-00833. The authors thank Dr. Qize He for his comments.

References

1. Rein G (2013) 9/11 world trade center attacks: lessons in fire safety engineering after the collapse of the towers. Fire Technol 49:583–585
2. Gann RG, et al (2005) Reconstruction of the fires in the world trade center towers. Federal building and fire safety investigation of the world trade center disaster. In: NIST NCSTAR, vol 1
3. Hu L, Milke JA, Merci B (2017) Special issue on fire safety of high-rise buildings. Fire Technol 53(1):1–3
4. Jin T (1978) Visibility through fire smoke. J Fire Flammabl 9(2):135–155
5. Jin T (2002) Visibility and human behavior in fire smoke. SFPE Handb Fire Prot Eng 3:2–42
6. Purser DA (2015) Combustion toxicity. In: Hurley MJ (ed) et alChp 62 SFPE handbook of fire protection engineering Springer, Berlin
7. Drysdale D (2011) An introduction to fire dynamics. Wiley, New York
8. Tamura GT (1970) Computer analysis of smoke movement in tall buildings. Division of Building Research, National Research Council, Ottawa
9. Klote JH (1989) Considerations of stack effect in building fires. National Institute of Standards and Technology, Gaithersburg

10. Walton G, Dols WS (2006) CONTAM 2.4 user guide and program documentation (No. NIST Interagency/Internal Report (NISTIR)-7251)
11. Qi D, Wang L, Zmeureanu R (2015) Modeling smoke movement in shafts during high-rise fires by a multizone airflow and energy network program. ASHRAE Trans 121:242
12. Black WZ (2009) Smoke movement in elevator shafts during a high-rise structural fire. Fire Saf J 44(2):168–182
13. Zhao G, Black W, Wang L (2017) Comparison of smoke management software and experimental measurements of smoke properties during a structural fire. In: ASHRAE 2017 winter conference
14. Wang LL, Black WZ, Zhao G (2013) Comparison of simulation programs for airflow and smoke movement during high-rise fires. ASHRAE Trans 119(2):1
15. Black WZ (2013) An integrated fire safety plan to manage smoke movement during a high-rise fire. ASHRAE Trans 119:146
16. Black WZ (2015) Stairwell pressurization and the movement of smoke during a high-rise fire. ASHRAE Trans 121:216
17. Black WZ (2010) COSMO—software for designing smoke control systems in high-rise buildings. Fire Saf J 45(6):337–348
18. Black WZ (2011) Computer modeling of stairwell pressurization to control smoke movement during a high-rise fire. ASHRAE Trans 117(1):1
19. Qi D, Wang L, Zmeureanu R (2014) An analytical model of heat and mass transfer through non-adiabatic high-rise shafts during fires. Int J Heat Mass Transf 72:585–594
20. Qi D, Wang L, Zmeureanu R (2017) The effects of non-uniform temperature distribution on neutral plane level in non-adiabatic high-rise shafts during fires. Fire Technol 53(1):153–172
21. Qi D (2016) Analytical modeling of fire smoke spread in high-rise buildings. Concordia University, Montreal
22. Qi D, Wang LL, Zhao G (2017) Froude-Stanton modeling of heat and mass transfer in large vertical spaces of high-rise buildings. Int J Heat Mass Transf 115:706–716
23. Zhang JY, Lu WZ, Huo R, Feng R (2008) A new model for determining neutral-plane position in shaft space of a building under fire situation. Build Environ 43(6):1101–1108
24. Zhang X, Wang S, Wang J, Giacomo R (2014) A simplified model to predict smoke movement in vertical shafts during a high-rise structural fire. J Eng Sci Technol Rev 7(2):29
25. Bae S, Ko GH, Lee CW, Ryou HS (2013) A network-based smoke control program with consideration of energy transfer in ultra-high-rise buildings, CAU_ESCAP. Build Simul 6(2):173–182
26. Chen Y, Zhou X, Fu Z, Zhang T, Cao B, Yang L (2016) Vertical temperature distributions in ventilation shafts during a fire. Exp Therm Fluid Sci 79:118–125
27. Hadjisophocleous G, Jia Q (2009) Comparison of FDS prediction of smoke movement in a 10-storey building with experimental data. Fire Technol 45(2):163–177
28. Acikyol BH, Balik G, Kilic A (2016) Experimental investigation of the effect of fire protection lobby on stair pressurization system in a high-rise building. Fire Technol 1(53):135–151
29. Strege S, Ferreira M (2016) Characterization of stack effect in high-rise buildings under winter conditions, including the impact of stairwell pressurization. Fire Technol 10:211
30. McGrattan K, Hostikka S, McDermott R, Floyd J, Weinschenk C, Overholt K (2013) Fire dynamics simulator, user's guide. NIST Spec Publ 1019:6th Edition
31. Quintiere JG (2006) Fundamentals of fire phenomena. Wiley Online Library, New York

32. Ohlemiller TJ, Mulholland GW, Maranghides A, Filliben JJ, Gann RG (2005) Federal building and fire safety investigation of the World Trade Center disaster: fire tests of single office workstations. NIST NCSTAR 1-5C. National Institute of Standards and Technology, Gaithersburg, MD
33. Karlsson B, Quintiere J (1999) Enclosure fire dynamics. CRC Press, Boca Raton
34. National Fire Protection Association (1995) 204M-guide for smoke and heat venting. Natl Fire Prot Assoc 995:1
35. He Q, Ezekoye OA, Tubbs B, Baldassarra C (2015) CFD simulation of smoke spread through elevator shafts during fires in high rise buildings. In: ASME 2015 international mechanical engineering congress and exposition, pp V08AT10A045–V08AT10A045
36. Committee AS et al (2013) ASHRAE handbook: fundamentals 2013. ASHRAE, Atlanta
37. Emmerich SJ, Persily AK (1998) Energy impacts of infiltration and ventilation in US office buildings using multi-zone airflow simulation. Proc IAQ Energy 98:191–206
38. Jeong JW, Firrantello J, Bahnfleth WP, Freihaut JD, Musser A (2008) Case studies of building envelope leakage measurement using an air-handler fan pressurisation approach. Build Serv Eng Res Technol 29(2):137–155
39. Klote JH, Ferreira MJ, Kashef A, Turnbull PG, Milke JA (2012) Handbook of smoke control engineering. American Society of Heating Refrigerating and Air-Conditioning Engineers, New Delhi
40. Tamura GT, Shaw CY (1976) Studies on exterior wall air tightness and air infiltration of tall buildings. ASHRAE Trans (United States) 82:122
41. Tamura GT, Shaw CY (1976) Air leakage data for the design of elevator and stair shaft pressurization systems. ASHRAE Trans 82(2):179–190
42. Tamura GT, Shaw CY (1978) Experimental studies of mechanical venting for smoke control in tall office buildings. Division of Building Research, National Research Council of Canada, Ottawa
43. McGrattan K, Hostikka S, McDermott R, Floyd J, Weinschenk C, Overholt K (2015) NIST special publication 1018-1, fire dynamics simulator (version 6.2) technical reference guide, volume 1: mathematical model. National Institute of Standards and Technology, Maryland
44. U.S. Nuclear Regulatory Commission (2016) Verification and validation of selected fire models for nuclear power plant applications: supplement 1. Office of Nuclear Regulatory Research (RES), Washington, DC and Electric Power Research Institute (EPRI), Palo Alto, CA. NUREG-1824 Supplement 1 and EPRI 3002002182
45. Bergman TL, Incropera FP, Lavine AS (2011) Fundamentals of heat and mass transfer. Wiley, New York
46. Babrauskas V (1989) Smoke and gas evolution rate measurements on fire-retarded plastics with the cone calorimeter. Fire Saf J 14(3):135–142
47. Babrauskas V, Krasny JF (2003) Upholstered furniture and mattresses. NFPA Fire Prot Handb Sect 8:1